Single-center model for double photoionization of the H_2 molecule

A. S. Kheifets*
Research School of Physical Sciences, The Australian National University, Canberra ACT 0200, Australia
(Received 15 June 2004; published 7 February 2005)

We present a single-center model of double photoionization (DPI) of the H_2 molecule which combines a multiconfiguration expansion of the molecular ground state with the convergent close-coupling description of the two-electron continuum. Because the single-center final-state wave function is only correct in the asymptotic region of large distances, the model cannot predict the magnitude of the DPI cross sections. However, we expect the model to account for the angular correlation in the two-electron continuum and to reproduce correctly the shape of the fully differential DPI cross sections. We test this assumption in kinematics of recent DPI experiments on the randomly oriented and fixed in space hydrogen molecule in the isotopic form of D_2.

DOI: 10.1103/PhysRevA.71.022704 PACS number(s): 32.80.Fb, 31.25.−v, 34.80.−i

I. INTRODUCTION

In recent years, remarkable progress has been achieved in experimental and theoretical studies of atomic and molecular double photoionization (DPI). The hydrogen molecule H_2, often substituted for experimental convenience by its heavier counterpart D_2, is a target of particular interest. The DPI process in H_2/D_2 is followed by the Coulomb explosion of the nuclei thus leading to the continuum state of four charged particles. Description of such a state is one of the most fundamental and challenging problems of the few-body physics.

Progressively sophisticated experimental techniques have been employed to study DPI of the hydrogen molecule. The first pioneering experiments [1,2] were performed by detecting photoion-photoion coincidences. In later experiments [3–7], electron-electron coincidence, or $(\gamma,2e)$ reaction, was implemented. On an earlier application of the cold target recoil momentum spectroscopy (COLTRIMS) technique [8], DPI from spatially aligned D_2 was measured by detecting one of the photoelectrons in coincidence with both fragment ions. In the latest COLTRIMS experiment [9,10], angular correlation of the two photoelectrons was measured thus facilitating the $(\gamma,2e)$ reaction on the fixed in space D_2.

On the theoretical side, several *ab initio* calculations [11–13] as well as empirical [14] and symmetry-driven [15,16] models have been reported for DPI on H_2. Despite these theoretical efforts, considerable amount of experimental data, especially the latest fully resolved differential cross sections (FDCS's), have not been reproduced in *ab initio* calculations. This gives us an incentive to develop a model which combines a central field expansion of the molecular ground state with the convergent close-coupling (CCC) description of the two-electron continuum. The CCC method proved to be predictive and reliable when applied to DPI of two-electron atomic targets: the He atom [17–19], its isoelectronic ion sequence [20], and alkaline-earth atoms [21]. It is therefore tempting to implement the CCC approach for DPI on H_2/D_2. In this case, however, we are confronted with a fundamental difficulty of dealing with a two-center nuclear potential. To circumvent this difficulty we may argue that the angular correlation in the two-electron continuum is established at large distances where the separation of the two nuclei can be neglected and they can be viewed as a united helium atom. As to the ground state, we have a choice of progressively accurate single-center expansions [22–25], the latter work claiming the chemical accuracy achieved for the ground-state energy. With the central-field approximation to the ground and final states, the application of the CCC method to molecular DPI is straightforward.

The single-center final state is incorrect in the vicinity of the nuclei where it overlaps with the molecular ground state and where the photoionization matrix elements gain their strength. Therefore we cannot expect the present model to produce accurate absolute DPI cross sections. However, we hope to reproduce correctly the shape of the DPI FDCS's. We have several reasons for hoping so. First, the $(\gamma,2e)$ experiments [3–5] revealed a close resemblance of the photoelectron angular correlation pattern in D_2 and He. This validates our assumption that the angular correlations in the two-electron continuum are not very different in He and the randomly oriented H_2/D_2. Second, asymptotic final states have been successful in describing shapes of DPI FDCS's in He. For instance, Maulbetsch and Briggs [26,27] employed a product of the three Coulomb (3C) functions to describe the He DPI FDCS's at both equal and unequal energy sharings between the photoelectrons. This is despite the fact that the 3C final state is incorrect in the vicinity of the nucleus and the magnitude of the FDCS is in error of several hundred percent [28]. And third, we can isolate separate terms in the CCC final state which are responsible for the magnitude and shape of the DPI FDCS. Indeed, we represent the final state by a close-coupling expansion over the two-electron channel states each of which is composed of a target bound state and a continuum state (see Sec. III for more detail). The bare photoionization matrix element is taken between the ground state and the final channel state. This bare matrix element is modified by an integral term which corresponds to an inelastic electron scattering on the singly ionized target. Due to a

*Electronic address: A.Kheifets@anu.edu.au;
URL: http://rsphysse.anu.edu.au/~ask107

TABLE I. Configuration mixing coefficients C_i and parameters of the Slater orbitals (n,l,ζ) for the ground state of H_2 at $R=1.4$ a.u.

i	N_1^i	N_2^i	C_i	N	n	l	n/ζ	N	n	l	n/ζ
1	1	1	0.195765	1	1	0	0.978	11	2	0	1.182
2	2	2	0.003276	2	1	0	0.752	12	1	0	1.122
3	2	3	0.581843	3	2	0	1.328	13	1	0	0.984
4	4	5	0.223090	4	2	0	1.598	14	1	0	1.024
5	5	5	−0.012841	5	3	0	0.876	15	2	0	1.170
6	6	7	−0.030708	6	1	0	0.876	16	3	2	1.374
7	6	8	0.007483	7	8	0	1.862	17	5	2	0.932
8	6	9	0.015074	8	11	0	1.830	18	8	2	1.538
9	10	16	0.128358	9	14	0	0.753	19	14	2	0.728
10	11	17	0.061705	10	1	0	0.978				
11	12	18	−0.023840								
12	12	19	0.013445								

long-range Coulomb interaction, this inelastic scattering in dominated by large impact parameters. We believe that it is the integral term which is responsible for the angular correlation in the continuum whereas the bare photoionization matrix elements control the overall magnitude of the DPI cross sections.

The rest of the paper is organized in the following way. In Sec. II we give the property of the single-center ground state. In Sec. III we outline the photoionization formalism. Results for the total and differential DPI cross sections are presented in Secs. IV A and IV B, respectively. The summary is given in Sec. V.

II. SINGLE-CENTER EXPANSION FOR THE GROUND STATE OF H_2

In the present model, we employ a single-center expansion for the ${}^1\Sigma_g^+$ ground state of the H_2 molecule proposed by Hayes [25]. The ground state is constructed as a configuration mixing of symmetrized pairs of the normalized Slater orbitals:

$$\phi_{nlm}(\boldsymbol{r},\zeta) = A(n,\zeta) r^{n-1} e^{-\zeta r} Y_{lm}(\boldsymbol{r}), \tag{1}$$

where the normalization coefficient $A(n,\zeta) = (2\zeta)^{n+1/2}[(2n)!]^{-1/2}$. The polar coordinates refer to the molecule midpoint. The full expansion given by Hayes [25] comprised 57 orbital pairs of $\{nlm,n'l'm'\}$ type with $m=-m'$ and $|m|\leqslant l$. Three sets of orbitals and configuration mixing coefficients were given for the internuclear separations of $R=1.2$, 1.4, and 1.6 a.u. The minimum of the ground-state energy −1.172 58 a.u. was found at a separation of 1.400 94 a.u.

For the purpose of numerical computations, we found that only few leading terms in the configuration mixing were essential. We restricted ourselves with 12 leading configurations built from 19 Slater orbitals which are listed in Table I. We label orbitals consequently with a single ordinal number N running from 1 to 19. For a given i configuration, a pair of numbers N_1^i, N_2^i denotes the relevant Slater orbitals and the configuration mixing coefficient C_i specifies the relative strength of this configuration.

Only axially symmetric orbitals with $m=0$ are selected in Table I. This simplifies angular momentum formalism and allows us to write the ground-state wave function in the following form:

$$\Psi_0(\boldsymbol{r}_1,\boldsymbol{r}_2) = \sum_{J_0} \sum_{nl,n'l'} N_{nl,n'l'} B_{nl,n'l'} \times \sum_{mm'} C^{J_0 M_0}_{lm,l'm'} \phi_{nlm}(\boldsymbol{r}_1)\phi_{n'l'm'}(\boldsymbol{r}_2). \tag{2}$$

In the above expression, the normalization factor $N_{nl,n'l'} = 2^{-1/2}\ (1+P_{12})$ for $nl \neq n'l'$ and $N_{nl,n'l'}=1$ otherwise, P_{12} denotes the spatial exchange operator. Since the Slater orbitals are not orthogonal for $l=l'$ and $n\neq n'$, we incorporated an extra overlap factor into $B_{nl,n'l'} = C_{nl,n'l'}(1 + |\langle n\zeta \| n'\zeta'\rangle|^2)^{-1/2}$, where $C_{nl,n'l'} \equiv C_i$ are configuration mixing coefficients listed in Table I and the radial overlap integral is calculated as

$$\langle n\zeta \| n'\zeta'\rangle = A(n,\zeta)A(n',\zeta')/A^2(\overline{n},\overline{\zeta})$$

with $2\overline{n} = n+n'$ and $2\overline{\zeta} = \zeta+\zeta'$. As is seen from Table I, at least one of the constituent orbitals in the configuration mixing always has an s orbital character whereas the second orbital is either s or d. Therefore the total angular momentum and its projection in the molecular ground state are $J_0=0,2$ and $M_0=0$. The Clebsch-Gordan coefficients entering Eq. (2) are $C^{00}_{00,00} = C^{20}_{00,20} = 1$.

III. MOLECULAR PHOTOIONIZATION FORMALISM

We align the $\boldsymbol{z}$ axis in the laboratory frame with the polarization vector of light $\boldsymbol{\varepsilon}$. The linear polarization along the $\boldsymbol{z}$ axis in the laboratory frame corresponds to two linear polarization components parallel and perpendicular to the molecular axis $\hat{\mathbf{R}}$. We calculate the dipole transition amplitude in the molecular frame and then transform it to the laboratory frame using the technique similar to that suggested by Feagin [14]. To deal with parallel and perpendicular polarizations, we introduce a two-electron dipole operator which corre-

sponds to a particular angular momentum projection of the photon M_P:

$$d(M_P) = \left(\frac{4\pi}{3}\right)^{1/2} [r_1 Y_{1M_P}(\hat{\mathbf{r}}_1) + r_2 Y_{1M_P}(\hat{\mathbf{r}}_2)]. \quad (3)$$

The two-electron dipole operators for the parallel and perpendicular polarization of light in the molecular frame can be expressed as $z_1+z_2=d(0)$ and $x_1+x_2=[d(-1)-d(1)]/\sqrt{2}$, respectively. In Eq. (3) the dipole operator is given in the length form. Analogous expressions in the velocity and acceleration forms can be obtained by substituting r_i with $\partial/\partial r_i$ and $2/r_i^3$, respectively.

In the CCC formalism, we represent the final state by a close-coupling expansion over the two-electron channel states each of which is composed of a target bound state f and a continuum state $\boldsymbol{k}$. To calculate the matrix element of the dipole operator (3) between the molecular ground state Ψ_0 and the channel state $|\boldsymbol{k}f\rangle$ we make a partial wave expansion over the angular momentum L and its projection M of the continuum state $\boldsymbol{k}$:

$$\langle \boldsymbol{k}f|d(M_P)|\Psi_0\rangle = \sum_{JM_J}\sum_{LM} i^{-L} e^{i\delta_L(k)} Y_{LM}(\boldsymbol{k}) C^{JM_J}_{LM,l_f m_f} (-1)^{M_P} \times \delta_{M_P+M_J,0} \langle kLn_f l_f \| d(M_P)\| \Psi_0\rangle. \quad (4)$$

Here we introduced the total angular momentum J and its projection M_J for the two-electron final state. In Eq. (4), the reduced dipole matrix element, free of electron angular momentum projections, is defined as

$$\begin{aligned}\langle kLn_f l_f \| d(M_P)\| \Psi_0\rangle = \sum_{J_0}\sum_{nl,n'l'} B_{nl,n'l} N_{nl,n'l'} \hat{J}\hat{J}_0 (-1)^{M_P} \\ \times \begin{pmatrix} J_0 & J & 1 \\ 0 & -M_P & M_P \end{pmatrix} \\ \times \Bigg[(-1)^{l_>} \sqrt{l_>} \langle kL\|r\|nl\rangle \langle n_f l_f \| l'n'\rangle \\ \times (-1)^l \begin{Bmatrix} J_0 & J & 1 \\ L & l & l_f \end{Bmatrix} \delta_{l'l_f} \\ + (-1)^{l_>} \sqrt{l_>} \langle n_f l_f \| r\| l'n'\rangle \langle kL\|nl\rangle \\ \times (-1)^{l'} \begin{Bmatrix} J_0 & J & 1 \\ l_f & l' & l \end{Bmatrix} \delta_{lL} \Bigg]. \end{aligned} \quad (5)$$

Here the hat symbol $\hat{J}$ denotes $(2J+1)^{1/2}$. For a spherically symmetric atomic target, $J_0=0$, $J=1$, and the matrix elements (5) are identical for all M_P. This is not the case for the molecular ground state (2) which has a substantial $J_0=2$ contribution. Because of this contribution there is a difference between the matrix elements (5) with $M_P=0$ and $M_P=1$. However, due to the axial symmetry of the ground state (2), the matrix elments with $M_P=\pm 1$ are identical.

We build the CCC final state from the two-electron channel states as

$$\Psi_f(\boldsymbol{k}) = |\boldsymbol{k}f\rangle + \sum_j \int\!\!\!\!\!\!\diagup d^3k' \frac{\langle \boldsymbol{k}f|T|j\boldsymbol{k}'\rangle |\boldsymbol{k}'j\rangle}{E - k'^2/2 - \epsilon_j + i0}. \quad (6)$$

Here $\langle \boldsymbol{k}f|T|j\boldsymbol{k}'\rangle$ is the half-on-shell T matrix which is found by solving a set of coupled Lippmann-Schwinger equations [29]. The dipole matrix element between the ground state Ψ_0 and the final state $\Psi_f(\boldsymbol{k})$ is given by

$$\langle \Psi_f(\boldsymbol{k})|d(M_P)|\Psi_0\rangle = \langle \boldsymbol{k}f|d(M_P)|\Psi_0\rangle + \sum_j \int\!\!\!\!\!\!\diagup d^3k' \times \frac{\langle \boldsymbol{k}f|T|j\boldsymbol{k}'\rangle \langle \boldsymbol{k}'j|d(M_P)|\Psi_0\rangle}{E - k'^2/2 - \epsilon_j + i0}. \quad (7)$$

We strip the angular dependence from the T matrix

$$\langle \boldsymbol{k}f|T|j\boldsymbol{k}'\rangle = \sum_{\substack{L,L',J \\ M,M',M_J}} C^{JM_J}_{LM,l_f m_f} C^{JM_J}_{L'M',l_j m_j} Y_{LM}(\boldsymbol{k}) Y^*_{L'M'}(\boldsymbol{k}') \times \langle kLn_f l_f \| T_J \| n_j l_j k'L'\rangle,$$

and perform the spherical integration and angular momentum projections' summation. This leads us to the following expression:

$$\begin{aligned}\langle \Psi_{Ln_f l_f}(k)\|D(M_P)\|\Psi_0\rangle \\ = \langle kLn_f l_f\|D(M_P)\|\Psi_0\rangle \\ + \sum_j \int\!\!\!\!\!\!\diagup_{k'} \frac{\langle kLn_f l_f\|T_J\|n_j l_j k'L'\rangle \langle k'L'n_j l_j\|D(M_P)\|\Psi_0\rangle}{E - k'^2/2 - \epsilon_j + i0}, \end{aligned} \quad (8)$$

where we introduced a complex phase-modified matrix element:

$$\langle kLn_f l_f\|D(M_P)\|\Psi_0\rangle = i^{-L} e^{i\delta_L(k)} \langle kLn_f l_f\|d(M_P)\|\Psi_0\rangle. \quad (9)$$

In the CCC formalism, a complete set of bound states $\{f\}$ is obtained by diagonalizing the target Hamiltonian and comprises both the positive and negative energy states. By projecting the positive energy bound state onto the true continuum state, we can access the doubly ionized continuum and to calculate the differential and total DPI cross sections. This technique is no different to the atomic DPI [17,18]. We write a dipole matrix element between the ground state and the two-electron continuum state as

$$\langle \Psi(\boldsymbol{k}_1,\boldsymbol{k}_2)|d(M_P)|\Psi_0\rangle = \sum_{JM}\sum_{l_1 l_2} \mathcal{Y}^{l_1 l_2}_{JM}(\hat{\mathbf{k}}_1,\hat{\mathbf{k}}_2) D_{l_1 l_2}(E_1 E_2) \times (-1)^{M_P} \delta_{M_P+M,0}. \quad (10)$$

Here we introduced bipolar harmonics [30],

$$\mathcal{Y}^{l_1 l_2}_{JM}(\hat{\mathbf{k}}_1,\hat{\mathbf{k}}_2) = \sum_{m_1 m_2} C^{JM}_{l_1 m_2, l_2 m_2} Y_{l_1 m_1}(\hat{\mathbf{k}}_1) Y_{l_2 m_2}(\hat{\mathbf{k}}_2).$$

The reduced matrix element is defined by the following projection:

$$D_{l_1 l_2}(E_1,E_2) = \langle \Psi_{l_1 n_2 l_2}(k_1)\|D(M_P)\|\Psi_0\rangle \langle l_2 k_2\|l_2 n_2\rangle, \quad (11)$$

where $\langle l_2 k_2\|l_2 n_2\rangle$ is the radial overlap between the pseudostate of energy $\epsilon_{n_2 l_2}=E_2$ and the true continuum radial wave function of same energy and angular momentum.

The nonspherically symmetric $J_0=2$ part of the ground state (2) can couple with the angular momentum of the photon to produce the two-electron final state with $J=1$ and 3. However, our numerical estimates show that the $J=3$ contribution to the matrix element (10) is small and we neglect it in the following. With this simplification, the angular momentum summation in Eq. (10) can be reduced to the sum over a single variable. By introducing symmetric and antisymmetric combinations of the radial matrix elements,

$$D^{\pm}_{l_1l_2}(E_1,E_2)=\frac{1}{2}\{D_{l_1l_2}(E_1,E_2)\pm D_{l_1l_2}(E_2,E_1)\}, \qquad (12)$$

we can write

$$\sum_{l_1l_2}\mathcal{Y}^{l_1l_2}_{1M}(\hat{\mathbf{k}}_1,\hat{\mathbf{k}}_2)D_{l_1l_2}(E_1E_2)=\sum_{l=0}^{\infty}D^{+}_{ll+1}(E_1,E_2)[\mathcal{Y}^{ll+1}_{1M}(\hat{\mathbf{k}}_1,\hat{\mathbf{k}}_2)+\mathcal{Y}^{ll+1}_{1M}(\hat{\mathbf{k}}_2,\hat{\mathbf{k}}_1)]+D^{-}_{ll+1}(E_1,E_2)\times[\mathcal{Y}^{ll+1}_{1M}(\hat{\mathbf{k}}_1,\hat{\mathbf{k}}_2)-\mathcal{Y}^{ll+1}_{1M}(\hat{\mathbf{k}}_2,\hat{\mathbf{k}}_1)].$$

The bipolar harmonics entering Eq. (13) can be evaluated by using the expression of Manakov *et al.* [31]:

$$\mathcal{Y}^{l_1l_2}_{1M}(\hat{\mathbf{k}}_1,\hat{\mathbf{k}}_2)=-\frac{1}{4\pi}\left(\frac{3}{l_{\max}}\right)^{1/2}[(-1)^{l_1}P'_{l_1}(\cos\theta_{12})(\hat{\mathbf{k}}_1)_M+(-1)^{l_2}P'_{l_2}(\cos\theta_{12})(\hat{\mathbf{k}}_2)_M], \qquad (13)$$

where $\cos\theta_{12}=(\hat{\mathbf{k}}_1\cdot\hat{\mathbf{k}}_2)$. This takes us to the following matrix elements for the parallel and perpendicular polarization:

$$\langle\Psi(\boldsymbol{k}_1,\boldsymbol{k}_2)|z_1+z_2|\Psi_0\rangle=(k_{1z}+k_{2z})g^{+}_{\Sigma}+(k_{1z}-k_{2z})g^{-}_{\Sigma}, \qquad (14)$$

$$\langle\Psi(\boldsymbol{k}_1,\boldsymbol{k}_2)|x_1+x_2|\Psi_0\rangle=(k_{1x}+k_{2x})g^{+}_{\Pi}+(k_{1x}-k_{2x})g^{-}_{\Pi}.$$

Here we introduced the symmetric and antisymmetric DPI amplitudes:

$$g^{\pm}_{\Sigma/\Pi}=\frac{\sqrt{3}}{4\pi}\sum_{l=0}^{\infty}\frac{(-1)^l}{\sqrt{l+1}}[P'_{l+1}(\cos\theta_{12})\mp P'_l(\cos\theta_{12})]\times D^{\pm}_{ll+1}(E_1,E_2), \qquad (15)$$

where indices Σ and Π correspond to the parallel ($M_P=0$) and perpendicular ($M_P=\pm1$) polarization of light, respectively. The M_P dependence is present, but not shown for brevity, in matrix elements (11) and (12).

Molecular frame expression (14) can be easily transformed to the laboratory frame. We give this expression for the case of equal energy sharing $E_1=E_2$ when we can simplify notations $g\equiv g^{+}$ since all g^{-} vanish:

$$\langle\Psi(\boldsymbol{k}_1,\boldsymbol{k}_2)|z_1+z_2|\Psi_0\rangle=(g_{\Sigma}\cos^2\theta_R+g_{\Pi}\sin^2\theta_R)(k_{1z}+k_{2z})+(g_{\Sigma}-g_{\Pi})\cos\theta_R\sin\theta_R(k_{1x}+k_{2x}). \qquad (16)$$

Here θ_R is the angle of the molecular axis relative to the polarization axis of light taken as the $\boldsymbol{z}$ axis in the laboratory frame. The two axes z and R form the xz plane in the laboratory frame, i.e., $\phi_R=0$.

Squared amplitude (16), with an appropriate kinematical factor, gives a FDCS of the DPI on a molecule fixed in space. An analogous expression for a randomly oriented molecule can be derived by introducing a nonzero polar angle ϕ_R into Eq. (16) and by taking the spherical integral over θ_R and ϕ_R. The resulting expression is given by Feagin [14]:

$$\frac{d\sigma^{2+}}{d\Omega_1d\Omega_2dE_2}=\frac{C}{15}\{[2|g_{\Sigma}|^2+7|g_{\Pi}|^2+6\,\mathrm{Re}(g_{\Sigma}f^{*}_{\Pi})](k_{1z}+k_{2z})^2+|g_{\Sigma}-g_{\Pi}|^2|\boldsymbol{k}_1+\boldsymbol{k}_2|^2\}. \qquad (17)$$

For a spherically symmetric atomic target, $g_{\Sigma}=g_{\Pi}$ and the second term in the right-hand side of Eqs. (16) and (17) cancels out. The proportionality constant depends on the gauge of the dipole operator. In the L gauge, $C=4\pi^2\omega/c$. Expressions (16) and (17) can be easily generalized to the case of an arbitrarily polarized light.

The total DPI cross section can be obtained by integrating the FDCS over the angles of the two photoelectrons and the energy of one of the photoelectrons. This, however, is a very inefficient computational procedure. Instead, we can use the completeness of the target states basis $\{f\}$ and obtain the total cross section as a sum over the positive energy target states. For a given momentum projection of the photon M_P, the photoionization cross section resolved with respect to the final target state f and the angle of emission of the photoelectron $\Omega_{\boldsymbol{k}}$ can be written as

$$\frac{d\sigma_{n_fl_f}(M_P)}{d\Omega_{\boldsymbol{k}}}=\frac{C}{3}\sum_{m_f}|\langle\Psi_f(\boldsymbol{k})|d(M_P)|\Psi_0\rangle|^2. \qquad (18)$$

The angle-integrated cross section is given by

$$\sigma_{n_fl_f}(M_P)=\frac{C}{3}\left|\sum_{L}\langle kLn_fl_f\|D(M_P)\|\Psi_0\rangle\right|^2. \qquad (19)$$

When transforming Eq. (19) to the laboratory frame, the perpendicular polarization component $\propto[D(-1)-D(1)]$ cancels out leaving us with the spherically symmetric component $D(0)$. The integration over the angular orientation of the molecular axis is performed trivialy. The total DPI cross section is given by the sum over all positive energy final states:

$$\sigma^{++}=\sum_{\epsilon_f>0}\sigma_{n_fl_f}(M_P=0). \qquad (20)$$

IV. RESULTS

A. Total DPI cross section

The total DPI cross section of H_2 calculated in three gauges of the dipole operator, the length, velocity, and acceleration, is presented in Fig. 1 in comparison with the experiment of Dujardin *et al.* [1] and a theoretical cross section reported by Le Rouzo [11]. Convergence between calculations in the three gauges is an indication of an accuracy of the ground- and final-state wave functions. A very good convergence can be achieved with the CCC final state for He

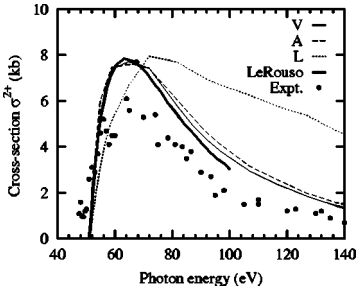

FIG. 1. Total DPI cross section calculated in three gauges of the dipole operator: length (L: dotted line), velocity (V: solid line), and acceleration (A: dashed line). Normalization is made to the calculation of Le Rouzo [11] in the *V* gauge (thick solid line) by dividing the present results by the factors of 20, 2.1, and 4.5 for the *L*, *V*, and *A* gauges, respectively. The experimental data by Dujardin *et al.* [1] are indicated by dots.

provided an accurate Hylleraas-type ground-state wave function is employed [32]. In a stark contrast, for the H_2 molecule all three gauges strongly diverge and the calculated cross section should be divided by various factors (20, 2.1, and 4.5 for the *L*, *V*, and *A* gauges, respectively) in order to normalize it to the absolute cross section reported by Le Rouzo [11]. After this renormalization, the *V* and *A* gauges agree well between each other and with the *V* gauge of Le Rouzo [11] whereas the *L* gauge shows a very different energy dependence.

This strong gauge divergence comes to us as no suprise. It is typical for asymptotically correct final states as was demonstrated by Lucey *et al.* [33] for the 3C final state in the case of DPI on He. What is surprising is a relatively good gauge convergence in the calculation of Le Rouzo [11]. Similarly to the present work, Le Rouzo [11] employed a multiconfiguration expansion of the H_2 ground state built from elliptical molecular orbitals. As to the final state, this author used a product of two Coulomb waves in the field of an asymptotic charge $Z=2$. We might envisage that the ground state employed by Le Rouzo [11] is somewhat superior to that of Hayes [25], even though the latter claims the chemical accuracy of the ground-state energy. As to the final state, the CCC wave function is certainly a better approximation than a completely noncorrelated product of the two Coulomb waves.

One more point should be made when discussing Fig. 1. Both the present calculation and that of Le Rouzo [11] completely ignore the vibrational degrees of freedom and correspond to the vertical double ionization energy of H_2 at 51.1 eV. The experimental DPI threshold is somewhat lower due to the Frank-Condon overlap between the vibrationally allowed part of the ground state and the strongly repulsive final state. Le Rouzo [12] addressed this question in a later work but we intentionally made a comparison with an earlier calculation of this author [11] which ignored this issue as we do in our model.

B. Differential cross section

Much of the renewed interest to DPI on H_2/D_2 is due to the recent accurate measurements of fully differential cross sections on randomly oriented [3–7] and fixed in space [9] molecular species. In this section we present our calculations for well documented cases of equal energy sharing kinematics at the total excess energies of 20 eV [3–5] and 24.5 eV [9].

1. Randomly oriented molecule

A triply differential cross section of DPI of H_2 for the kinematics of experiment of Reddish *et al.* [3] is shown in Fig. 2. In this coplanar kinematics the two photoelectrons and the polarization vector of light all belong to the same plane. The escape angles of the photoelectrons θ_1 (fixed) and θ_2 (variable) are counted from the polarization axis of light (horizontal in polar plots of Fig. 2).

Two different calculations are presented in Fig. 2. In the first calculation Eq. (17) is used with two amplitudes g_Σ and g_Π [Eq. (15)] corresponding to the parallel and perpendicular orientation of the molecular axis relative to the polarization of light. To show clearly the role of the molecular effects, in the second calculation we only use one amplitude g_Σ and the second amplitude is set to be identical $g_\Pi \equiv g_\Sigma$.

Molecular effects due to the second term in the right-hand side of Eq. (15) should be especially noticeable when the fixed photoelectron escape angle θ_1 deviates from 90°. The atomic-like term in Eq. (15) forbids the two-electron escape on the cone about the polarization *z* axis where $k_{1z}=-k_{2z}$. It suppresses one of the lobes in atomiclike FDCS's (dashed

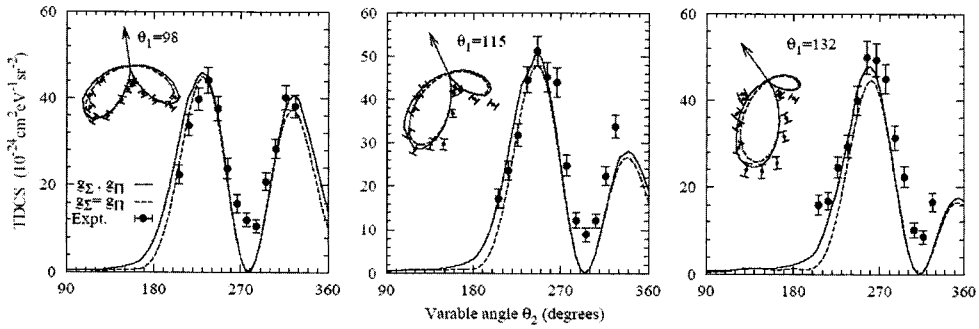

FIG. 2. Triply differential cross section of DPI on H_2 at $E_1=E_2=10$ eV and a coplanar kinematics. A *V*-gauge calculation with amplitudes g_Σ and g_Π [Eq. (15)] is displayed by a solid line. An atomiclike calculation with identical amplitudes $g_\Sigma=g_\Pi$ is shown by a dashed line. A fixed escape angle of one of the photoelectrons is indicated by an arrow on the inset polar plots. The polarization axis of light is horizontal. Experimental data are from Wightman *et al.* [5]

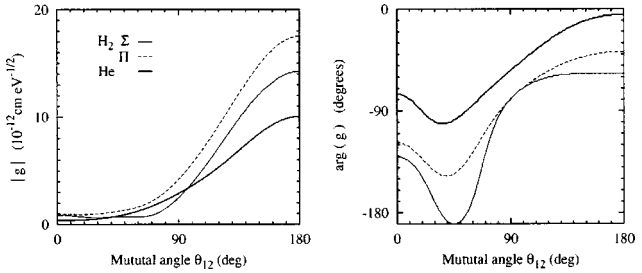

FIG. 3. The DPI amplitudes g_Σ, g_Π for H_2 are shown by the solid and dashed lines, respectively. Their atomic counterparts $g_\Sigma = g_\Pi$ for He are displayed by the thick solid line. The moduli are on the left panel and the phases are on the right panel.

line in Fig. 2) when the direction of escape of one of the photoelectrons becomes close to the polarization axis. The molecular term only forbids the antiparallel escape $\boldsymbol{k}_1 = -\boldsymbol{k}_2$ and enforces just one nodal point. That is why the lobes should be more symmetric in the molecular case when both terms contribute in Eq. (15) (solid line in Fig. 2). The experimental data seem to show this tendency. However, the theoretical difference between the molecular g_Σ, g_Π and atomic-like $g_\Sigma = g_\Pi$ calculations is too small. The filling of the antiparallel escape node is most likely due to a finite angular resolution ($\pm 2.5°$) and other experimental effects.

It is instructive to compare the H_2 DPI amplitudes g_Π, g_Σ with those for the He atom. This comparison is made in Fig. 3. The amplitudes (left) and their phases (right) are plotted as functions of the mutual angle of the two photoelectrons θ_{12}.

It is also interesting to compare the presently calculated amplitudes with those introduced empirically by Feagin [14] to fit the experimental data of Wightman *et al.* [5]. Feagin [14] considered a pair of *real* amplitudes g_Σ, g_Π in the Gaussian ansatz,

$$g_{\Sigma,\Pi} \propto \exp\left[-2 \ln 2 \frac{(\pi - \theta_{12})^2}{\Delta\theta_{12}^2} \right], \tag{21}$$

and treated the ratio g_Π/g_Σ and width $\Delta\theta_{12}$ as two adjustable parameters. The best fit to the experiment of Wightman *et al.* [5] was achieved at $g_\Pi/g_\Sigma = -2.1 \pm 0.5$ and $\Delta\theta_{12} = 76° \pm 3°$.

In the present calculation, the amplitudes are complex. However, inspection of Fig. 3 shows that the phase difference between g_Σ and g_Π is close to zero for those mutual angles θ_{12} where the magnitude of the amplitudes is significant. A small phase difference can be accommodated by a real g_Π/g_Σ ratio. Fitting with the Gaussian ansatz (21) produces the width parameters $\Delta\theta_{12}^\Sigma = 84°$, $\Delta\theta_{12}^\Pi = 88°$, and the amplitude ratio $g_\Pi/g_\Sigma = 1.2$.[1] For comparison, the He width parameter is 91°. The difference between the width parameters in He and H_2 is the sole ground-state effect since the CCC final states are identical in both calculations. We investigated numerical stability of the Gaussian parameters by varying the size of the CCC basis. The Gaussian parameters were not very stable with the width changing by as much as ±5°. However, in all cases we observed that $\Delta\theta_{12}^\Sigma < \Delta\theta_{12}^\Pi < \Delta\theta_{12}^{\mathrm{He}}$.

We note that the molecular effects are weak in our model. The g_Π/g_Σ ratio differs from unity by only 20%. This is consistent with the angular composition of the ground state given in Table I which has about the same amount of the *d* orbital character. In contrast, the amplitude ratio of Feagin [14] is very far from unity and points to strong molecular effects.

2. Molecule fixed in space

Recent COLTRIMS measurements of Weber *et al.* [9] allowed the extraction of FDCS's at particular orientations of the molecular axis rather than averaged over all possible orientations. In addition, these authors were able to determine FDCS's at various energies of the recoiling ions [10]. Due to the Frank-Condon principle, these measurements probe the molecular ground state at various internuclear separations. Hayes [25] gave the multiconfiguration expansion of the H_2 ground state at three different internuclear distances of $R = 1.2$, 1.4, and 1.6 atomic units. By employing these ground-state expansions we should be able, at least in part, to reproduce the evolution of the FDCS's as the molecule expands or shrinks.

In Fig. 4 we present our calculation for the case of an H_2 molecule being fixed in the plane of the coplanar $(\gamma, 2e)$ reaction. Both photoelectrons, polarization axis of light, and the molecular axis all lie in the same plane. The escape angle of one photoelectron is fixed at $\theta_1 = 10°$ relative to the polarization axis of light (horizontal in Fig. 4). In the top-left panel, all molecular orientations are taken into account whereas in other panels the molecular axis angle θ_R varies from 15° to 90° relative to the polarization of light.

According to Eq. (16), the g_Σ amplitude dominates the FDCS when $\theta_R \simeq 0$ whereas the g_π amplitude makes the sole contribution when $\theta_R = 90°$. In intermediate cases both amplitudes interfere. As $g_\Pi > g_\Sigma$, we see an increase of the magnitude of the FDCS when θ_R varies from small angles towards 90°. However, due to the interference, the FDCS peaks not at 90° but at a somewhat lesser angle of 60°. The pure Π-FDCS at 90° clearly shows an extra lobe which is also pronounced in the spherically averaged FDCS. Comparison is made with experimental data of Weber [34]. The spherically averaged experiment clearly shows a two-lobe structure, in agreement with the present calculation. However, the additional lobe is much broader and the node at the antiparallel emission of the two photoelectrons is significantly filled in. This is probably due a finite angular resolution of the experiment which also combines with a finite energy partition acceptance. These factors cannot be accounted for in the present calculation. However, simulation of the finite angular and energy resolutions with Gaussian amplitudes (21) significantly improves agreement between calculated and measured FDCS [9]. Experimental data presented in Fig. 4 show the increase of the magnitude as predicted by the present calculation. However, at small θ_R angles, the shape of the FDCS is much more isotropic and the magnitude is far too small. It is unlikely that these effects

[1] We introduced an additional phase factor $(-1)^{M_P}$ both to the amplitude (4) and the reduced matrix element (5). Without this factor, the ratio g_Π/g_Σ would be negative as reported in Weber *et al.* [9]

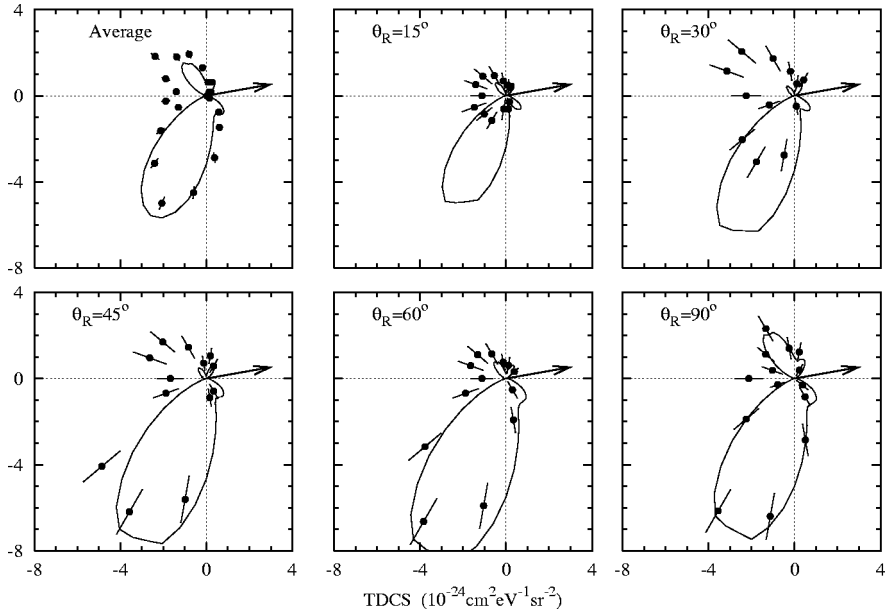

FIG. 4. Triply differential cross section of DPI on H_2 at $E_1=E_2=12.5$ eV and a coplanar kinematics. The fixed photoelectron escape direction at $\theta_1=10°$ is indicated by an arrow. The top-left panel shows the FDCS averaged over all molecular orientations. Other panels correspond to a fixed molecular angle θ_R relative to the polarization of light (horizontal). A *V*-gauge calculation with amplitudes g_Σ and g_Π [Eq. (15)] is displayed by a solid line. Experimental data are from Weber [34].

are solely due to finite experimental resolutions, rather the limited scope of the present model may cause this disagreement.

Finally, in Fig. 5 we present the FDCS for perpendicular geometry of the two-electron escape when one of the photoelectrons is detected at 90° to the plane formed by the polarization axis of light and the internuclear axis of the molecule. The second electron is detected in this plane at various angles relative to the polarization axis of light. The molecule forms an angle $\theta_R=55°$ relative to this axis. The central panel of Fig. 5 corresponds to the equilibrium internuclear distance $R=1.4$ a.u. whereas on the left and right panels this distance is 1.6 and 1.2 a.u., respectively. The experimental data of Weber *et al.* [10] shown in each panel are taken at different kinetic energy release (KER) values. Due to the Frank-Condon principle and because of a strongly repulsive doubly ionized final state, the smaller KER values correspond to the expanded molecule (left panel), and the larger KER value is a signature of a shrunk molecule (right panel).

The calculation is in a good agreement with experiment at the equilibrium internuclear distance (central panel). However, there are some obvious features on the experimental FDCS which are not reproduced by the calculation. We would expect the present central-field model to fail sooner for an expanded molecule (left panel). Much to our surprise, it is the shrunk molecule which generates the most unusual four-lobe FDCS. We stress that Eq. (16) can only describe a two-lobe FDCS as a function of the photoelectron angle θ_2 in the present geometry. It is higher multipoles, most notably $J=3$ in the final two-electron continuum, that cause such a strong deviation from a dipole two-lobe FDCS. The present model indicates some reduction in magnitude of the FDCS at smaller internuclear separations, in line with experiment. However, the $J=3$ final channels are far too small to account for a nondipole structure of the FDCS.

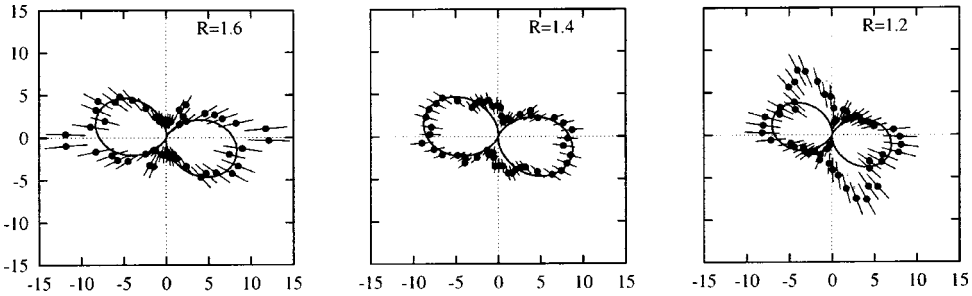

FIG. 5. Triply differential cross section of DPI on H_2 at $E_1=E_2=12.5$ eV and noncoplanar geometry. The fixed escape direction of one of the photoelectrons is perpendicular to the plane which contains the polarization of light, the molecule which is at 55° to the polarization axis, and the escape direction of another photoelectron. The experimental data are from Weber *et al.* [10].

V. CONCLUSIONS

We presented here a formalism and numerical results for the one-photon two-electron ionization of the H_2 molecule within a simplified single-center model. The model combines a multiconfiguration expansion for the molecular ground state and a convergent close-coupling (CCC) expansion for an atomiclike final state in which the two photoelectrons move in a field of a pointlike $Z=2$ charge. Electron correlation is accounted for both in the ground and final states.

We generated a succession of cross sections, starting with the total integrated DPI cross section, followed by the fully differential cross section for a randomly oriented H_2 molecule and, finally, the FDCS for a molecule fixed in space. We made a comparison with the latest experimental data and, where available, with previous calculations. We find our model modestly accurate. Due to an asymptotic nature of the final state, we do not expect accurate magnitudes of the calculated DPI cross sections. In addition, the total DPI cross section shows great sensitivity to the gauge of the electromagnetic operator, the velocity gauge being the closest to the experiment and giving the most accurate photon energy dependence. The shapes of the FDCS for randomly oriented H_2 molecules is found in fair agreement with experiment [5,9]. Narrowing of the Gaussian width of the parallel and perpendicular DPI amplitudes as compared with the fully symmetric He amplitude is shown unambiguously. The effects of the molecular axis orientation and the internuclear separation on the FDCS are demonstrated within the present model. However, certain important features of the experimental FDCS such as strong deviation from a two-lobe dipole structure [10] cannot be reproduced.

In general, the molecular effects are rather weak in the present model as expected from a small fraction of the *d*-orbital character in the multiconfiguration ground state [25]. This character does not change appreciably as the internuclear distance deviates from the equilibrium. The possible $J=3$ final channels are too weak to explain nondipole features of the FDCS.

To improve the accuracy of the present model, it would be highly desirable to include the molecular effects in the final state. This can be achieved in the prolate spheroidal coordinates as was demonstrated by Semenov and Cherepkov [35] in their calculation of the single photoionization cross section of H_2. We plan this development of our model in the future.

ACKNOWLEDGMENTS

The author wishes to thank Bedros Joulakian who gave some valuable advice at initial stages of this project. The help of Igor Bray is greatly appreciated in maintaining the helium CCC code. The author benefited significantly from numerous stimulating discussions with Thorsten Weber and Reinhard Dorner. Dr. Weber is particularly acknowledged for supplying experimental data prior to publication. The bulk of the computations were performed using the Compaq AlphaServer SC National Facility of the Australian Partnership for Advanced Computing.

[1] G. Dujardin, M. J. Besnard, L. Hellner, and Y. Malinovitch, Phys. Rev. A **35**, 5012 (1987).
[2] H. Kossmann, O. Schwarzkopf, B. Kämmerling, and V. Schmidt, Phys. Rev. Lett. **63**, 2040 (1989).
[3] T. J. Reddish, J. P. Wightman, M. A. MacDonald, and S. Cvejanović, Phys. Rev. Lett. **79**, 2438 (1997).
[4] N. Scherer, H. Lörch, and V. Schmidt, J. Phys. B **31**, L817 (1998).
[5] J. P. Wightman, S. Cvejanović, and T. J. Reddish, J. Phys. B **31**, 1753 (1998).
[6] S. A. Collins, A. Huetz, T. J. Reddish, D. P. Seccombe, and K. Soejima, Phys. Rev. A **64**, 062706 (2001).
[7] D. P. Seccombe, S. A. Collins, T. J. Reddish, P. Selles, L. Malegat, A. K. Kazansky, and A. Huetz, J. Phys. B **35**, 3767 (2002).
[8] R. Dörner *et al.*, Phys. Rev. Lett. **81**, 5776 (1998).
[9] T. Weber *et al.*, Phys. Rev. Lett. **92**, 163001 (2004).
[10] T. Weber *et al.*, Nature (London) **431**, 737 (2004).
[11] H. Le Rouzo, J. Phys. B **19**, L677 (1986).
[12] H. Le Rouzo, Phys. Rev. A **37**, 1512 (1988).
[13] M. Walter and J. Briggs, J. Phys. B **32**, 2487 (1999).
[14] J. M. Feagin, J. Phys. B **31**, L729 (1998).
[15] T. J. Reddish and J. M. Feagin, J. Phys. B **32**, 2473 (1999).
[16] M. Walter and J. S. Briggs, Phys. Rev. Lett. **85**, 1630 (2000).
[17] A. S. Kheifets and I. Bray, Phys. Rev. A **54**, R995 (1996).
[18] A. S. Kheifets and I. Bray, J. Phys. B **31**, L447 (1998).
[19] A. S. Kheifets and I. Bray, Phys. Rev. Lett. **81**, 4588 (1998).
[20] A. S. Kheifets and I. Bray, Phys. Rev. A **58**, 4501 (1998).
[21] A. S. Kheifets and I. Bray, Phys. Rev. A **65**, 012710 (2002).
[22] H. W. Joy and R. G. Parr, J. Chem. Phys. **28**, 448 (1958).
[23] S. Hagstrom and H. Shull, J. Chem. Phys. **30**, 1314 (1959).
[24] S. Hagstrom and H. Shull, Rev. Mod. Phys. **35**, 624 (1963).
[25] E. F. Hayes, J. Chem. Phys. **46**, 4004 (1967).
[26] O. Schwarzkopf, B. Krassig, V. Schmidt, F. Maulbetsch, and J. S. Briggs, J. Phys. B **27**, L347 (1994).
[27] F. Maulbetsch and J. S. Briggs, J. Phys. B **26**, L647 (1993).
[28] M. Pont and R. Shakeshaft, Phys. Rev. A **51**, R2676 (1995).
[29] I. Bray and A. T. Stelbovics, Adv. At., Mol., Opt. Phys. **35**, 209 (1995).
[30] D. A. Varshalovich, *Quantum Theory of Angular Momentum*, 1st ed. (World Scientific, Philadelphia, 1988).
[31] N. L. Manakov, S. I. Marmo, and A. V. Meremianin, J. Phys. B **29**, 2711 (1996).
[32] A. S. Kheifets and I. Bray, Phys. Rev. A **57**, 2590 (1998).
[33] S. P. Lucey, J. Rasch, C. T. Whelan, and H. R. J. Walters, J. Phys. B **31**, 1237 (1998).
[34] T. Weber, Ph.D. thesis, Institut für Kernphysik, Universität Frankfurt, 2003.
[35] S. K. Semenov and N. A. Cherepkov, Chem. Phys. Lett. **291**, 375 (1998).